Proceedings of ASME Turbo Expo 2019
Turbomachinery Technical Conference and Exhibition
GT2019
June 17-21, 2019, Phoenix, Arizona, USA

GT2019-90938

INVESTIGATING INSTABILITIES IN A ROTATING DETONATION COMBUSTOR OPERATING WITH NATURAL GAS-HYDROGEN FUEL BLEND – EFFECT OF AIR PREHEAT AND ANNULUS WIDTH

Arnab Roy[1,2], Clinton Bedick[1], Donald Ferguson[1], Todd Sidwell[1], Peter Strakey[1]

[1]National Energy Technology Laboratory, Morgantown, West Virginia 26507

[2]West Virginia University Research Corporation, Morgantown, West Virginia 26505

ABSTRACT

Propagation characteristics of a detonation wave in an air-breathing Rotating Detonation Combustor (RDC) using natural gas-hydrogen fuel blends is presented in this paper. Short duration (~up to 6s) experiments were performed on a 152.4mm OD uncooled RDC with two different annulus gap widths (5.08mm and 7.62mm) over a range of equivalence ratios (0.6-1.0) at varying inlet air temperatures (~65°C-204°C) and natural gas content (up to 15%) with pre-combustion operating pressure slightly above ambient.

It was observed that the RDC, with an annulus gap width of 5.08mm, was inherently unstable when natural gas (NG) was added to the hydrogen fuel while operating at pre-combustion pressures near ambient and at an inlet air temperature of 65°C. Increasing the annulus gap width to 7.62mm improved the stability of the detonation wave at similar temperatures and pressure permitting operation with as much as 5% NG by volume. While observed speeds of the detonation waves were still below theoretical values, an increase in inlet air temperature reduced the variability in wave speed. The frequency analysis thus explored in this study is an effort to quantify detonation instability in an RDC under varying operational envelope. The data presented is relevant towards developing strategies to sustain a stable detonation wave in an RDC using natural gas for land based power generation.

INTRODUCTION

Gas turbine engines account for nearly 30% of the domestic electricity generation and improvements in thermal efficiency are often pursued by elevating the turbine inlet temperatures. This approach has resulted in incremental improvements with today's state of the art combined cycle plant achieving slightly over 63% [1]. However, material properties and cooling requirements ultimately limit the maximum sustainable temperatures in both the combustor and turbine. An alternative approach could be realized through pressure gain combustion in which the post-combustion, total pressure is greater than the compressor exit pressure. Both deflagrative and detonative technologies have been considered for pressure gain combustion applications, but unlike deflagration, detonative technologies have the potential advantage of significantly increasing pressure following the Zeldovich-von Neumann-Doring (ZND) process while maintaining high combustion exit temperatures. Rotating Detonation Engines / Combustion (RDE/RDC) is one form of pressure gain combustion device that is being considered. Like other pressure gain combustion devices, RDC's produce an inherently unsteady flow. The periodic unsteadiness of the flow provides for predictable behaviors however under certain operating conditions the detonation can become unstable. Understanding the mechanisms behind unstable modes is critical to the development of the combustor and ultimately to expanding its operating regime.

BACKGROUND STUDY

Anand, *et al*. [2] classify four fundamental instabilities in RDCs, many of which have also been observed by other researchers. The first is, aperiodic chaotic propagation within the combustion annulus due to operation near lean limits, with subsonic air injection, or with large fuel injection orifices [2–

4]. It is suggested that this phenomena can be characterized by incoherent pressure-time traces, which may imply numerous failure and re-initiation events as the detonation wave propagates [2,5]. The second instability is a low-frequency sinusoidal oscillation, characterized by "waxing and waning" of detonation peak pressures [2]. Additionally, modulation of amplitude and frequency may be observed within the air and fuel plenums [6,7]. Ultimately, it is suggested that this may be attributed to the constructive/destructive interference between shocks from current and previous detonation waves and is expected to depend strongly on the reactant injection scheme [6,8]. Third is the well-known mode-switching phenomena [2,9–11], in which a sudden change in wave direction or number of waves occurs. It has been proposed that a greater number of waves within the annulus may be preferable for stable operation [2]. The final instability is that of axisymmetric pulsed operation [2,12], which has been observed during backpressure operation. It has been theorized that this instability may be due to shock-reflections from the RDC exit followed by shock-initiation of fresh reactants. In ref. [2], this pulsed detonation mode was observed at ~3.8kHz.

Most research RDCs implement hydrogen as a fuel due to ease of detonability. For a given fuel-oxidizer mixture, this is often characterized by cell size [13]. A detonation cell structure is formed by shock-boundary and shock-shock interactions as the high temperature and pressure reaction front propagates through the mixture [13,14]. This leads to the development of transverse waves and the formation of shock intersection triple points and Mach stems, which give way to the classical diamond-shaped cell structure [13,14]. In un-confined detonations, the cell structure is believed to correspond to the "true" detonability limits of a particular mixture, depending only on the initial gas state [14]. In this instance, the dimensions of the cell structure are expected to be tied directly to the chemical induction length (or time) [13]. However, the detonability limits of confined mixtures may depend strongly on the boundary conditions of the medium in which the detonation propagates [14]. The effect of these boundary conditions will result in a minimum geometric criteria to achieve sustained or stable detonation, which has been shown to be a function of the cell size [13,14].

It has been suggested that fill height, in addition to annulus width [3,15,16], may represent an important characteristic dimension affecting detonability in RDCs. Similar to other geometric requirements, this translates to fitting some minimum number of cells within the height of the detonation wave front. Fill height can be approximated using Eq. 1, which represents the axial distance traveled by the reactant mixture in the time between two successive waves. Here, $\dot{m}$ is the total reactant mass flow rate, ρ_{mix} is the reactant mixture density, f_{RDC} is the RDC operating frequency, and $A_{annulus}$ is the flow area of the combustion annulus in the axial direction. In this simple comparison, it is assumed that any number of waves are equally distributed along the circumference of the RDC and that the reactants are uniformly mixed. Additionally, details such as flow choking, injector dynamics, or property affects due to turbulence and rapid expansion are neglected.

$$h_{fill} = \frac{\dot{m}}{\rho_{mix} f_{RDE} A_{annulus}} \quad [1]$$

Experimental cell size data exist for numerous fuel/oxidizer/diluent combinations, as well as various initial temperatures and pressures [13,14,17]. In general, the cell size reaches a minima at stoichiometric conditions, with a u-shaped curve extending toward richer and leaner compositions. For hydrogen-air, this corresponds to a minimum cell size of ~10-15mm at standard temperature and pressure [13,14,17]. Increasing the initial temperature (and/or pressure) tends to decrease cell size. For power generation applications, operation with natural gas and air is paramount to achieving widespread implementation of RDC and PGC technologies. Unfortunately, natural gas (~methane), exhibits one of the largest cell sizes of the hydrocarbon fuels, corresponding to ~200-350mm for a stoichiometric mixture at standard temperature and pressure [17,18]. As this paper focuses specifically on hydrogen-methane-air mixtures, cell size data for single component fuels are of limited applicability. Currently, a single reference has been identified [19], which contains experimental cell size data for hydrogen-methane mixtures, up to 50% methane by volume, as a function of equivalence ratio. The characteristic u-shaped curve is maintained, however it narrows considerably with higher methane concentrations.

For the reasons outlined above, most published research on RDE/RDC's has focused on hydrogen-air mixtures. However, there has been some recent work to extend operation to more practical hydrocarbon fuels. A few research efforts [15,20–22] have had success in detonating ethylene-air mixtures within an RDC, however not without significantly greater challenges than for hydrogen. This may be attributed to increased mixing times compared to hydrogen [21], as well as fundamental limits associated with detonation cell size [17]. Wilhite *et al.* [15] initially failed to detonate ethylene air mixtures in a conventional annular RDC, but later achieved successful detonations in a centerbody-less design [20]. This was largely attributed to a reduction in quenching effects from the large heat transfer area of the confined annular channel. Second, improved consistency/stability was observed for higher air flow rates. Wang *et al.* [21] demonstrated some success in a more conventional annular RDC configuration, noting instabilities related to lean limits and wave bifurcation, similar to hydrogen fueled RDCs. Similar to Wilhite *et al.* [15] , higher air flow rates appeared to improve consistency and stability. Zhong *et al.* [22] were able to achieve detonation with an ethylene-acetylene-hydrogen mixture. It was noted that increasing proportions of ethylene and acetylene hindered the operational range of the RDC, consistent with the relative detonability limits of the fuel components [17]. Of particular note was self-ignition of fresh reactants ahead of the detonation wave, thereby weakening the propagating detonation wave. It was

suggested that this phenomena lead to thermo-acoustic interactions which manifest as operational instabilities [22].

Still fewer researchers have had success detonating methane (~natural gas) in air, presumably due to the significantly increased cell size. This is an important milestone for the development of RDE/RDC technologies for land-based power generation applications. An intermediate step, which may provide the necessary experience and data to further develop natural gas fueled RDCs, is to implement customized fuel blends. For example, Schwer *et al.* [24] has conducted a computational study on the effects of various fuel blends on detonability and RDC performance. It was shown that for methane as a fuel, even a small amount of a more reactive fuel such as hydrogen, can reduce the induction time by as much as a factor of ten, thereby allowing detonation to be achieved. Bykovski *et al.* [25] applied a similar approach to experimental testing of an RDC with methane-hydrogen fuel blends (in air). Here, a ~500mm RDC was utilized and hydrogen volume fractions from ~40-90% were implemented. As the methane fraction was increased the range of operable equivalence ratios shrank from ~0.78-1.56 to ~1.0-1.23, with combustion extending outside of the annular gap for the highest methane fraction. Welch and Tobias *et al.* [26,27] studied a methane fueled RDC using enriched air (i.e. oxygen volume fraction > 21%). Stable operation was achieved for an oxygen volumetric fraction of 70% and stoichiometric proportions of fuel and oxidizer, although wave speed fluctuations on the order of ±200 m/s were observed. Walters *et al.* [28] attempted to operate an RDC using methane and air at elevated inlet temperatures and backpressure in an effort to reduce the size of the detonation cell. While the authors were unable to achieve detonation, their analysis illustrated that the targeted temperature and pressure (600K and 20atm), should reduce the cell size sufficiently to permit detonation within an RDC annulus for a methane-air mixture.

The present study is an effort to investigate the instabilities observed in a lab scale RDC operation with natural gas-hydrogen-air mixtures and to emphasize the effect of annulus gap size and inlet air temperature on detonation wave stability.

EXPERIMENTAL METHODS

NETL RDC Test Facility

Figure 1 shows the RDC test rig integrated into the high pressure Low Emission Combustor Test and Research (LECTR) facility at the National Energy Technology Laboratory (NETL). The RDC geometry is based on a previous design by the Air Force Research Laboratory (AFRL). While the internal geometries and dimensions of the AFRL and NETL design are largely identical, the NETL RDC was modified to enable integration with the NETL facility, specifically, for operation at elevated back-pressure and for the addition of instrumentation ports in the fuel and air plena. Two variants of annulus gap sizes were used for this study where 5.08mm is the original (nominal) design size and 7.62mm is the enlarged version. The combustor is uncooled and thus individual tests are limited to 6-10 seconds of run time to prevent overheating. The NETL facility is currently configured to enable RDC operation at pre-combustion pressures up to 1.76MPa with active control and measurement of combustion air and fuel flow rates.

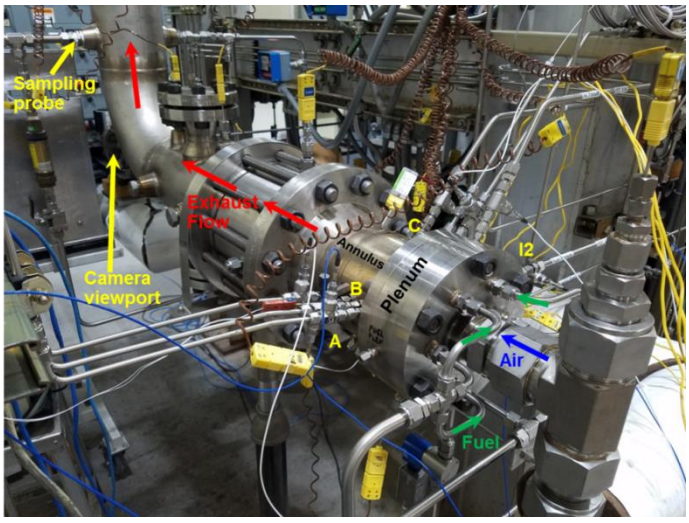

(a)

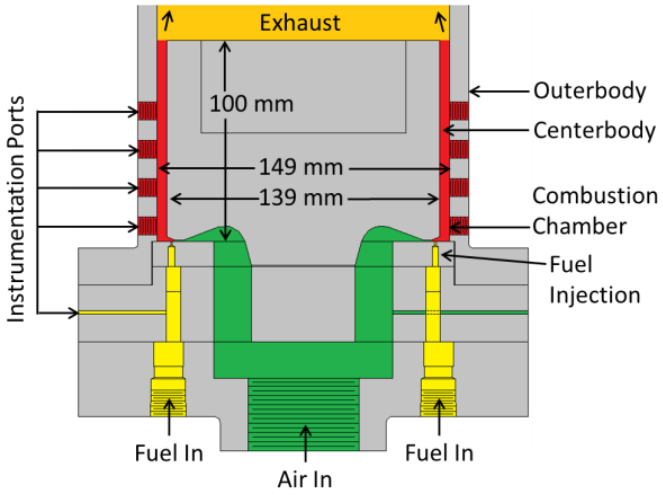

(b)

Figure 1: RDC Test Setup at NETL (a) Test Facility, (b) RDC design

Combustion air can be provided with a maximum flow rate of 1.15kg/s at a maximum pre-heat temperature of 425°C (although temperatures were limited to 200°C to protect sensitive instrumentation). The RDC can be fueled by mixtures of hydrogen and natural gas, which are available at maximum flow rates of 13g/s and 55g/s, respectively. The RDC discharges into an enclosed exhaust section and the initial pressure in the RDC and exhaust sections can be established by

high-temperature back pressure control valves installed at the end of the exhaust section. Process conditions (such as fuel and air flow rates, process pressure and process temperature) are measured by traditional methods (Coriolis mass flow and differential pressure meters, pressure transducers and thermocouples) and are controlled and recorded by the process control system (Allen-Bradley ControlLogix PLCs and Siemens Wonderware HMI.) High-speed pressure data (up to 1MHz) and wall thermocouple temperature data (2Hz) collection is performed through an independent LabView-based National Instruments data acquisition system. Additional sample gas extraction ports are available in the exhaust section that can be connected directly to gas analyzers for emission measurements (NOx, O_2, CO etc.). The horizontally-mounted configuration enables optical access to the RDC annulus along the combustor axis through a 25.4mm (1inch) diameter quartz viewport installed in the elbow section downstream of the RDC exhaust, which is utilized for high speed imaging of the detonation wave.

Instrumentation, Data Acquisition and Operation

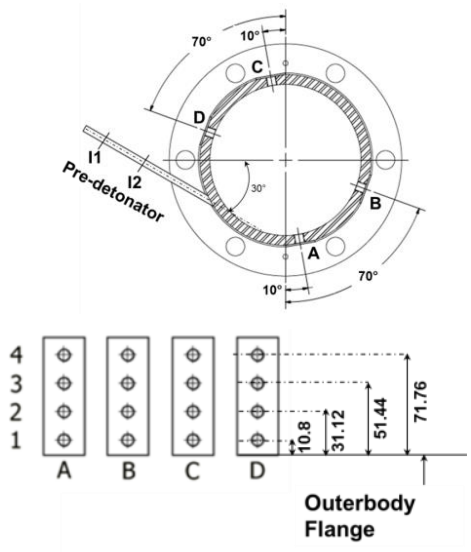

Figure 2: NETL RDC instrumentation nomenclature

The RDC is instrumented to measure the variation in dynamic and static pressure along axial as well as circumferential directions as shown in Fig. 2 and Table 1. Dynamic pressure is measured by piezoelectric pressure transducers mounted in an Infinite Tube Pressure probe (ITP) configuration in which the transducer is mounted approximately 50mm away from the apparatus in a tee junction with a long length (~5meters) of 6.35mm OD (¼ inch) stainless steel tubing extending from the tee. These probes are fast response dynamic pressure transducers from CA102B and 113B series manufactured by PCB® Piezotronics with high temperature ablative coating. This configuration provides some temperature protection for the probe while reducing ringing effects from the shock waves. From Naples *et al.* [29] it is understood that ITP mounted pressure transducers do not accurately measure the pressure amplitude compared to a transducer directly exposed to the detonation, however the focus of this experimental effort is to utilize the dynamic pressure to characterize the detonation wave speed (compared to theoretical Chapman-Jouguet (CJ) wave speed as determined by ZND model) and not the absolute magnitude of pressure in the combustor. A fiber optic probe is used in the detonation plane (C2) to measure OH* chemiluminescence. This probe is a 1000micron (fused silica with Aluminum buffer) UV/VIS multimode temperature resistant (Model#UVV10-39SMA) fiber optic cable manufactured by Accuglass Products Inc. housed inside a ¼" tubing as shown in Fig. 1 and is air cooled near the tip. The probe collects light from the reaction front of the detonation wave and passes through a filter (310nm) and is incident on a Photo-multiplier tube (PMT). The output of the PMT generates voltage spikes after each wave passing and thus the reaction front of a periodic detonation wave rotating around the annulus can be identified. It is important to mention here that due to harsh detonation environment the fiber optic probe though recessed from the annulus outer-body wall sees the flame front directly, may deteriorate in signal strength with repeated runs or even during a single run with longer test duration before it is eventually damaged and no signal could be collected. Therefore, the OH* signals reported in this paper will be used for temporal resolution only, however no comparison of the strength or intensity of the peaks between cases will be used for discussion as the amplitudes have not been calibrated.

The transducers mounted on the air and fuel plenum measure the low amplitude oscillation that is important in characterizing the injection dynamics and detonation wave interaction. The thermocouples measure the RDC outer-body wall temperature at three different depths along the same axial location and the data can be utilized for 1-D transient heat flux calculations. The dynamic pressure transducer in the initiator fuel line acts as a trigger for timing the spark and other process control parameters as shown in Fig. 3.

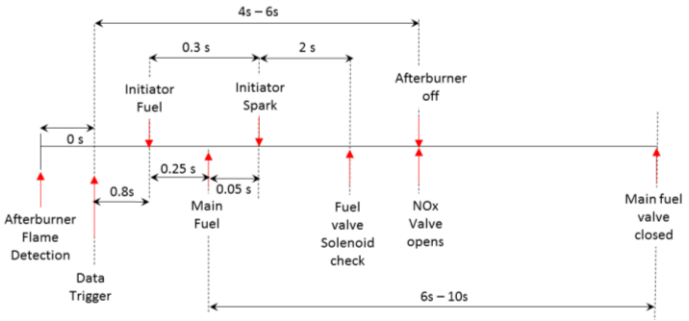

Figure 3: RDC operational timing diagram

Figure 3 shows the timing sequence for a typical RDC experiment. The entire sequential process starts with ignition of an afterburner.

Table 1: RDC Instrumentation and Data Acquisition

Port#	Measurement	Sampling Rate	Instrument	Uncertainty
I1/I2	Dynamic Pressure	250kHz	PCB (ITP)	+/-1.3%, RS<0.1us, RF>500kHz
A1/A4	Static Pressure	250kHz	Kulite (CTAP)	+/-5%
B1/B2/B4/C1	Dynamic Pressure	250kHz	PCB (ITP)	+/-1.3%, RS<0.1us, RF>500kHz
C2	OH* signal	250kHz	Optical Fiber	
C4	Static Pressure	250kHz/2Hz	Rosemount PT (stand-off)	
Fuel/Air Plenum	Dynamic Pressure	250kHz	PCB	+/-1.3%, RS<0.1us, RF>500kHz
Initiator Fuel	Dynamic Pressure	250kHz	PCB	+/-1.3%, RS<0.1us, RF>500kHz
Exhaust-1/2	Dynamic Pressure	100kHz	Kistler	+/-5%
D1/D4-1-3	Wall Temperature	2Hz	K Type TC	
-	Flow rate, Plenum pressure	2Hz	Coriolis Flow meter, Differential PT	NG=+/-0.35%, H_2=+/-5%, Air=+/-2%

RS = Rise Time, RF = Resonant Frequency

Table 2: RDC Test Cases

Annulus Width (mm)	Flow Rates (m^3/s)	Eq. Ratio	Preheat (°C)	Back Pressure (kPa)	Natural Gas (volume % in fuel)
5.08	Air: 0.35 ± 0.01	0.95 ± 0.05	65/121	atm.	0-15%
7.62	Air: 0.35 ± 0.01	0.95 ± 0.05	65/121	atm.	0-15%
7.62	Total: 0.47 ± 0.01	0.6/1.0	65/204	atm.	0-15%

The afterburner consists of two opposing, horizontally-mounted (east and west), radially-injected torches located roughly 0.5m downstream of the RDC exit plane. The afterburner torches are fueled by a near-stoichiometric natural gas-air mixture and the flame is anchored to the injectors using a bluff body. Only when the afterburner flame is detected on both east and west sides, the data trigger becomes active and starts the data acquisition as well as the initiator ignition sequence. The initiator fuel valve is timed to open after 0.8s of data trigger and the initiator spark follows subsequently. After a series of experiments, it was found that 0.25s-0.3s of delay to fire the initiator spark is the optimum for achieving detonation in the initiator.

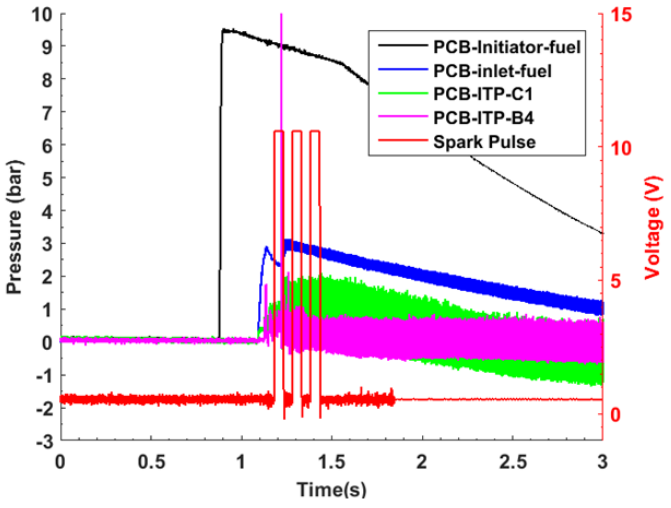

Figure 4: Sequence of RDC operation – high speed data acquisition

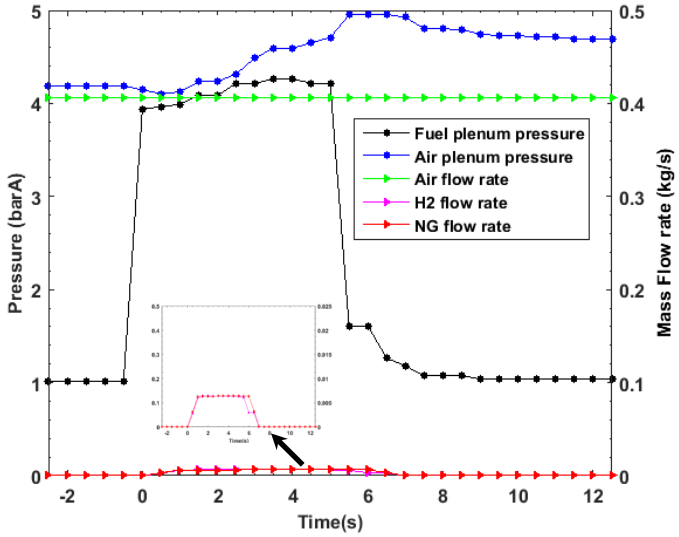

Figure 5: Operating conditions for a specific RDC test run for natural gas content=10%, phi=0.8, 204°C air temperature and atmospheric exhaust pressure

There is an additional solenoid valve installed in the main fuel line upstream of the RDC that closes as a safety measure if the thermocouple located between RDC exhaust and afterburner does not register temperatures higher than a threshold set for combustion. This is to prevent excess unburnt fuel-air mixture entering the exhaust sections in case of a failed detonation attempt. The duration of afterburner operation is typically set to 4s-6s, however it can be further reduced.

Figure 4 shows a snapshot of high speed data acquisition (250 kHz) for the first 3s of a successful detonation event after

the data trigger is received (t=0) following the operational sequence as illustrated in Fig. 3. The pressure spike recorded by the PCB during the initial transient is representative of the von Neumann pressure spike from an overdriven stoichiometric hydrogen-air detonation in the ignition tube. Here a detonation wave is generated in the stoichiometric mixture by a spark-plug in order to initiate detonation in the primary combustor. The spark is fired three times within 0.3s time in a controlled manner in order to attempt RDC ignition. It has also been observed that the addition of the afterburner has a significant effect on RDC startup which has been reported in earlier experiments [30]. Figure 5 shows the fuel and air flow rates at an upstream location and static pressure measured at the plenum respectively.

RESULTS AND DISCUSSION

The experimental results discussed in this section emphasize on RDC performance using pure hydrogen and in presence of natural gas premixed with hydrogen at 5% concentration respectively and is presented in the following manner – first, effect of annulus size on RDC characteristics have been explored near stoichiometric mixture condition for nominal (65°C) and intermediate (121°C) air preheat. This is followed by highlighting the overall wave speed distribution obtained under different air preheat levels (65°C/121°C/204°C) for the larger annulus gap (7.62mm) ranging from lean (phi ~ 0.6) to stoichiometric conditions. Finally detailed insight of instabilities and identifying important characteristics of RDC operation is presented under stoichiometric mixture conditions at nominal and highest air preheat temperatures. All case studies have been compared while operating with pure hydrogen and hydrogen-NG blend. Additionally, further insight is provided to better explore the detonation instability and understanding of the complex wave speed characteristics using detonation cell size correlation and prediction. Table-2 summarizes the RDC operating conditions and test cases presented in this paper.

Effect of annulus gap width on RDC operation with and without natural gas addition

Figure 6 shows a comparative study of hydrogen-air RDC operation for two annulus gap sizes, where the raw signal obtained from the dynamic pressure transducer at C1 and OH* chemiluminescence probe at C2. Both PCB and OH* signals are processed through Butterworth filter between 100Hz to 20kHz to remove thermal drift (PCB) and associated noise (both) at undesired frequencies to obtain corresponding spectrogram plots (Fig. 6(a)-(b),(d)-(e)). The time t=0 is marked when the initiator spark is fired and data is shown according to the duration of the RDC test run (3s or 5s). Finally the dominant frequencies w.r.t time are highlighted in Figs. 6(c),(f) for the two annulus gap size cases from which the wave speed distribution could be calculated. The spectrogram data shows abrupt change in frequency modes for both annulus gap widths, where for the larger annulus the transition happens earlier (~1.25s) compared to the smaller annulus (~4.2s) during the test window. However, the data suggests that for the smaller annulus the frequency change corresponds to a shift in operational mode from 2-wave (~7.25kHz) to a 3-wave (~10.3kHz) homogeneous rotation. This is evident from the sharp dominant frequency observed in both Figs. 6(a) and (c). The other frequency lines observed in both C1 and OH* spectrogram are lower and upper harmonics of fundamental frequency only. This is in contrast to the characteristics observed in case of 7.62mm annulus where the data from C1 signal suggests a decrease in dominant frequency and the corresponding wave speed, whereas the dominant frequency obtained from the OH* signal undergoes a mode change after ~1.2s of startup. This is a distinctive feature observed for the larger annulus not seen for the smaller (nominal) counterpart at 65°C. This phenomenon may suggest de-coupling of the reaction front from the shock wave and is discussed later. The OH* signal spectrum for 7.62mm annulus also seems noisy and broadened around the dominant frequency. This typically indicates additional instability of the detonation wave and may lead to further bifurcation mode where wave fronts may be randomly colliding with each other. To further explore the detonation propagation characteristics, two time windows (t1=0.5s and t2=2s) are selected from Fig. 6(a) and (d) and the dynamic pressure/OH* data and is investigated in details as shown in Fig. 7.

Figure 7 (a)-(h) represents dynamic pressure data filtered between 100Hz and 20kHz measured at different axial locations (B1-B2-B4 for 5.08mm and B1-B2-B3-B4 for 7.62mm annulus gap) illustrating several distinct characteristic features and compares the relative magnitudes at the same reference level during each test window of 1ms each. The raw PCB data at C1 and OH* chemiluminescence signal (C2) is also shown for the entire test window for reference. The PCB transducers even if installed in the ITP configuration, show significant amount of thermal drift especially in the detonation plane. Comparing the pressure peaks in the axial direction, it can be observed that the time difference between B1-B2 peaks is much narrower in case of the larger annulus for both time windows. This indicates that the detonation wave front is more orthogonal or less skewed. It is also interesting to note that the sequence of the B1-B2 peak (larger amplitude peaks) reverses at a later stage (t2=2s) for the 7.62mm annulus case which is not observed for the 5.08mm annulus gap. This trend could be useful to determine the direction of skewness of the detonation wave in the axial direction. There is also a notable difference in terms of the relative peak magnitudes of B1-B2 between the two annulus cases. For 7.62mm annulus the B1-B2 peaks are almost similar in magnitude suggesting the detonation strength is uniform across the wave height (or fill height) and exists at least up to the location of the B2 instrumentation port. The B1-B2 peaks are distinctly different in case of the smaller annulus and shows reduced intensity near B2.

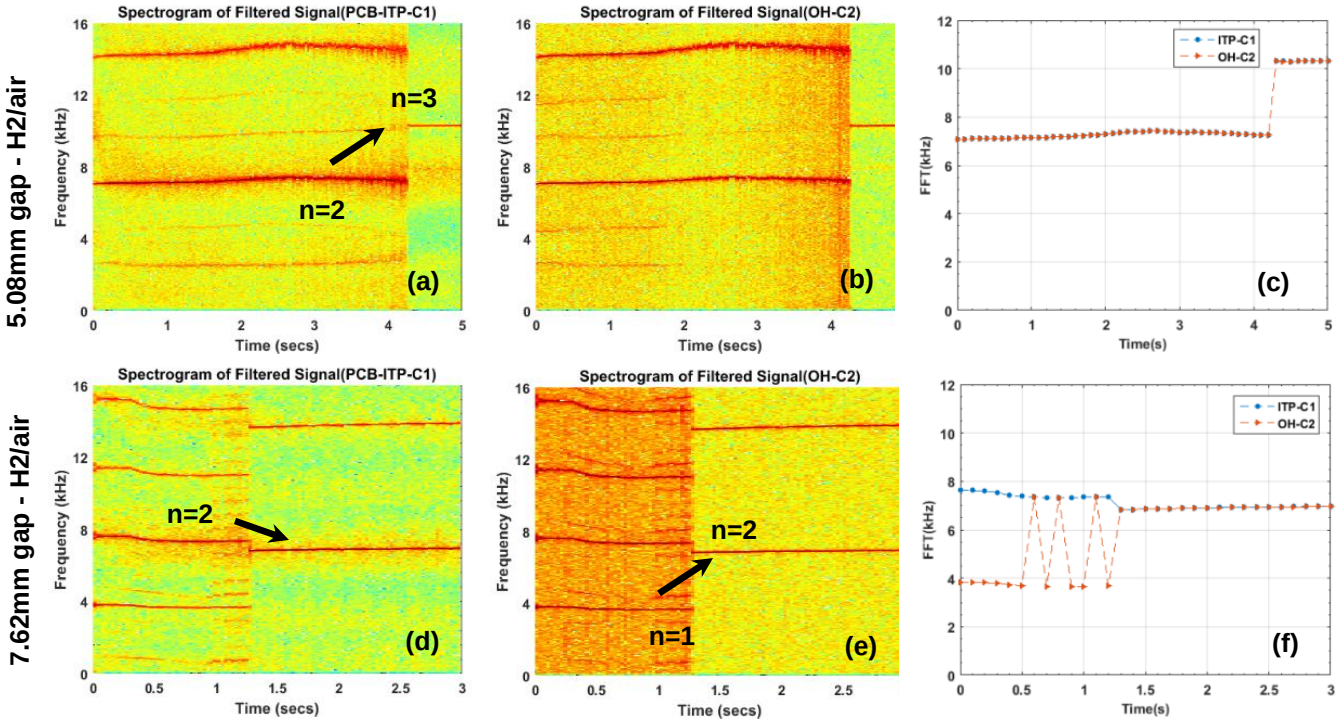

Figure 6: Effect of annulus size (5.08mm (top) vs 7.62mm (bottom)) on RDC performance for pure hydrogen-air operation at, phi~0.95, 65°C air temperature, 0.35m^3/s (STP) air flow rate and atmospheric exhaust pressure – Spectrogram of ITP-C1 (left) and OH* signal (middle) filtered between 100Hz and 20kHz, and dominant frequency distribution w.r.t. test duration obtained from PCB-C1 and OH* (right)

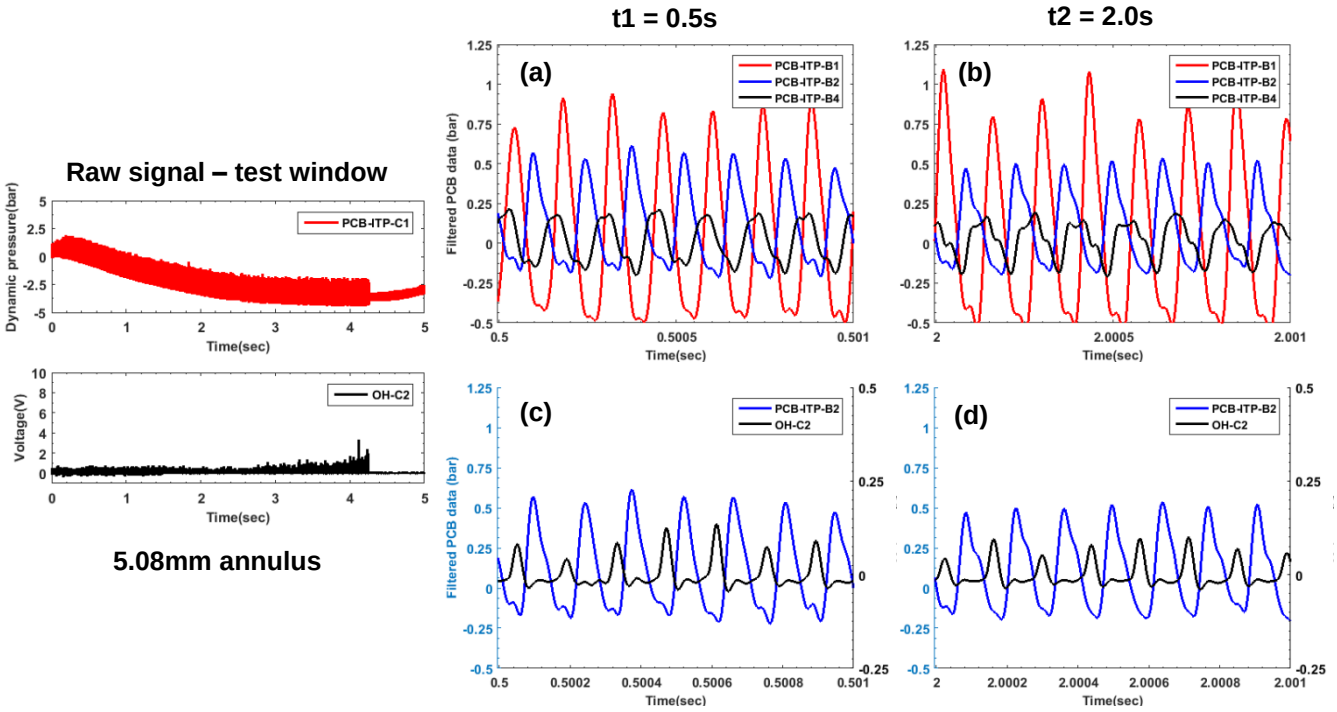

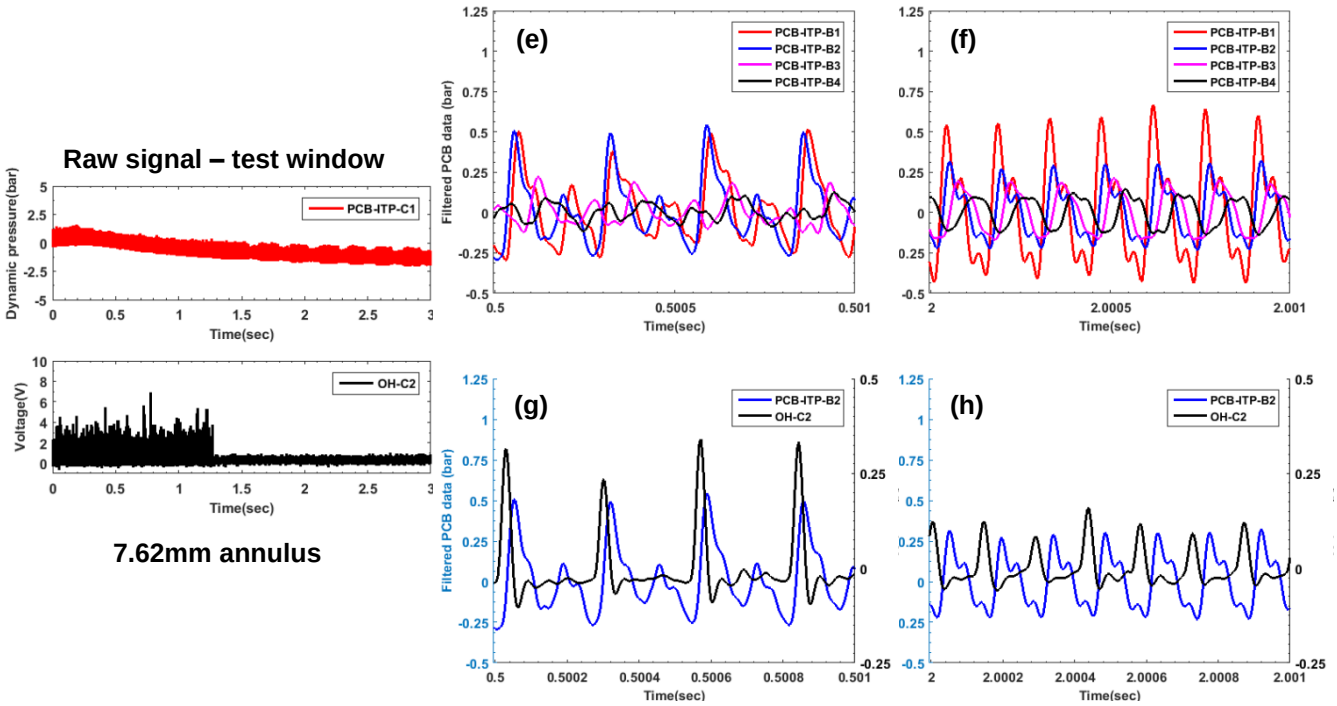

Figure 7: Effect of annulus gap width – raw signal (PCB-C1 and OH*-C2) measured during full test window and close-up view of dynamic pressure trace measured at B1, B2, B3 and B4 and B2, OH* signal respectively at different instants (t1=0.5s and t2=2s) during the test window under conditions as shown in Fig. 6

Investigating this trend, it could be speculated that the detonation wave height may be larger in case of 7.62mm annulus gap width compared to 5.08mm. Figures 7(c)-(d), (g)-(h) provide a useful insight on detonation wave and reaction front coupling by looking at dynamic pressure signals and OH* probe chemiluminescence at same axial location (B2 and C2) but different circumferential planes. It is expected that a peak in the dynamic pressure signal could arise due to either the leading shock wave of a detonation front or an individual shock wave only. However, a periodic peak in OH* chemiluminescence on the other hand would suggest stronger heat release due to reaction zone from a detonation wave only, as it has been observed that for pure deflagration there is almost no signal obtained due to significant difference in heat release rate. Pure deflagration cases can also be identified by a combination of absence of strong peaks in PCB data, FFT of the PCB dynamic pressure signal leading to a very low wave speed (typically <40% CJ speed) and wall thermocouple data which hardly shows any temperature rise. The coupling or decoupling of the heat release region from the detonation wave could therefore be identified by looking at the sequence of the measured data. For the smaller annulus and both time windows, t1=0.5s and t2=2s, it can be seen that every peak of B2 is followed by a peak of OH*. However, for the larger annulus double peaks in PCB-B2 signal are observed followed by a corresponding single OH* peak. This indicates the presence of a pure shock wave of lesser strength compared to the leading shock wave of the detonation front that may not have transitioned into a detonation wave within the specific time window. However, at a later stage t2=2s, it seems a secondary detonation wave front has formed from the pure shock wave as evident from the one to one correlation between B2 and OH* signal peaks. The overall amplitude of the pressure oscillation is reduced, leading to lower detonation wave strength and reduced frequency. The phase sequence between B2-OH* peaks can also be utilized to quantify induction length of the detonation wave.

It is to be noted here that for 5.08mm annulus gap size configuration, attempts to initiate and/or to sustain detonation were unsuccessful even with the smallest amount of natural gas addition (2.5%) in the hydrogen stream at nominal inlet air temperature of 65°C operating at pre-combustion pressures near atmospheric. Therefore, to highlight the effect of annulus size on RDC performance in presence of natural gas, another test case study is considered where the characteristics are compared at a higher air preheat (121°C) temperature near stoichiometric operation with 5% NG content in the fuel stream with hydrogen as shown in Fig. 8.

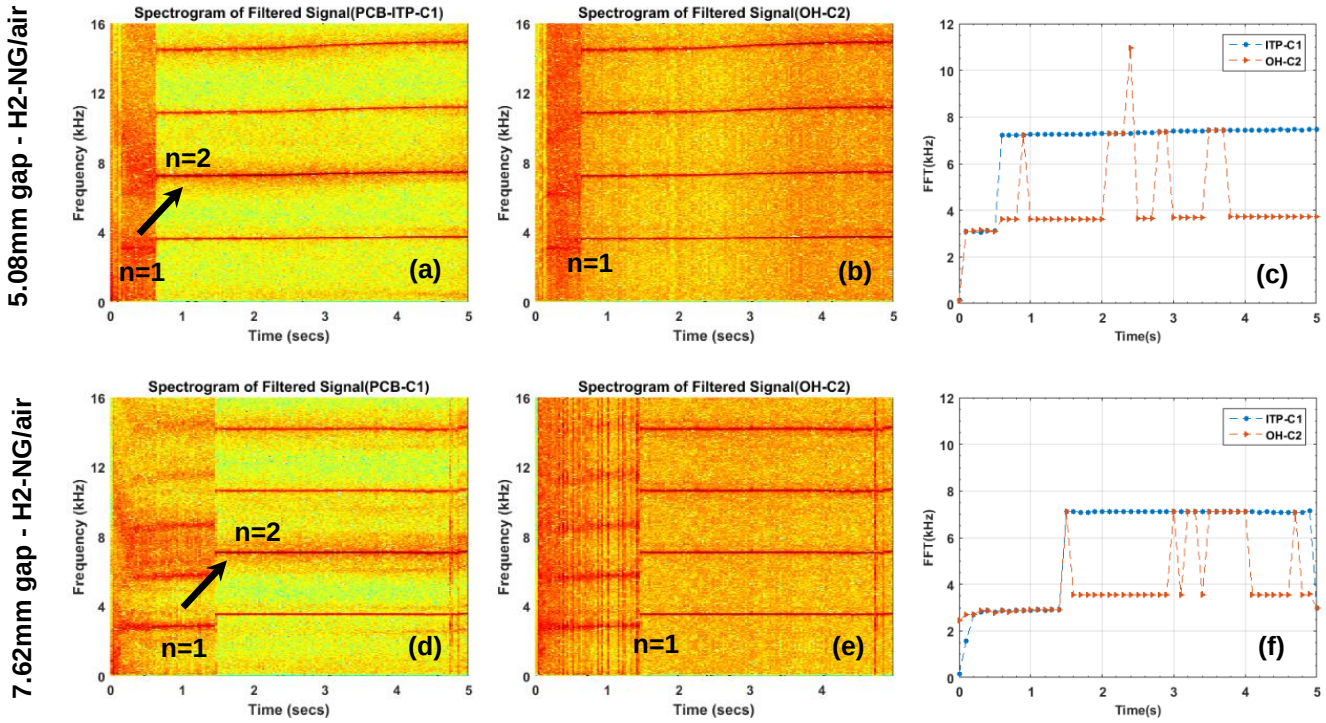

Figure 8: Effect of annulus size (5.08mm (top) vs 7.62mm (bottom)) on RDC performance for hydrogen-natural gas blend air operation at, NG content = 5%, phi~0.9, 121°C air temperature, 0.35m^3/s (STP) air flow rate and atmospheric exhaust pressure – Spectrogram of ITP-C1 (left) and OH* signal (middle) filtered between 100Hz and 20kHz, and dominant frequency distribution w.r.t. test duration obtained from PCB-C1 and OH* (right)

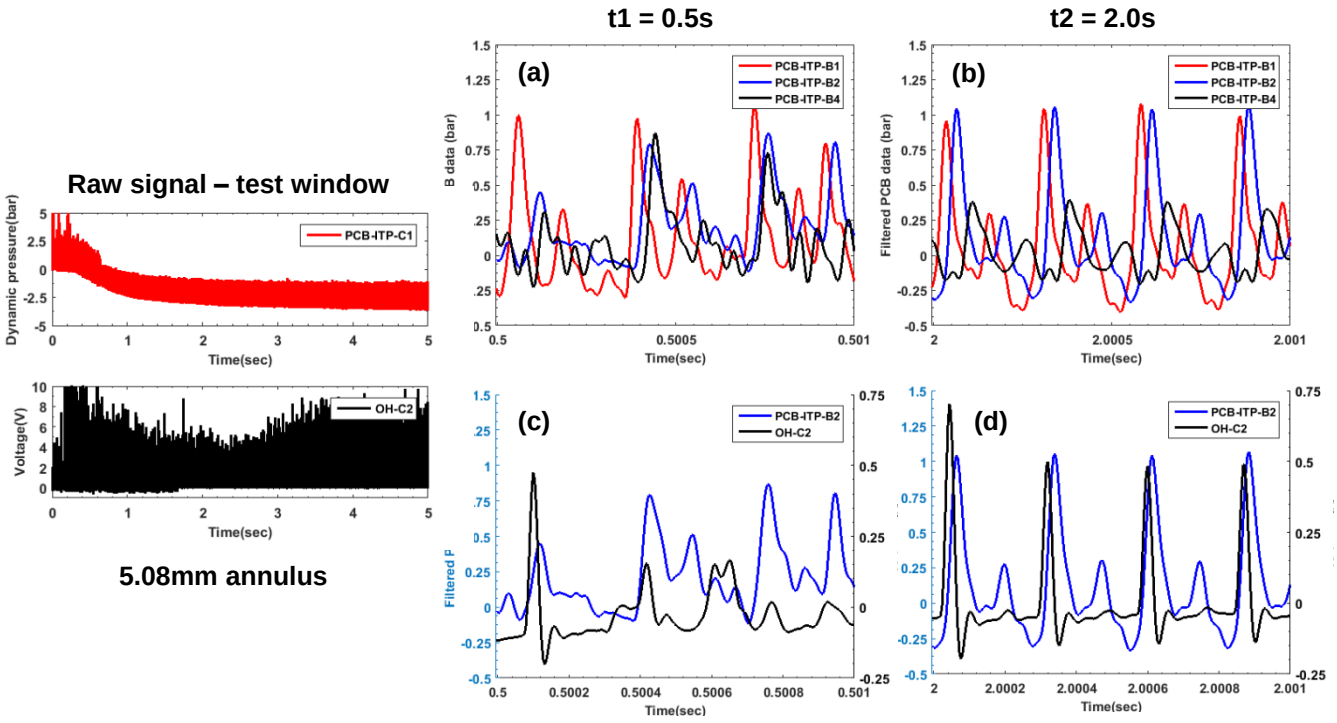

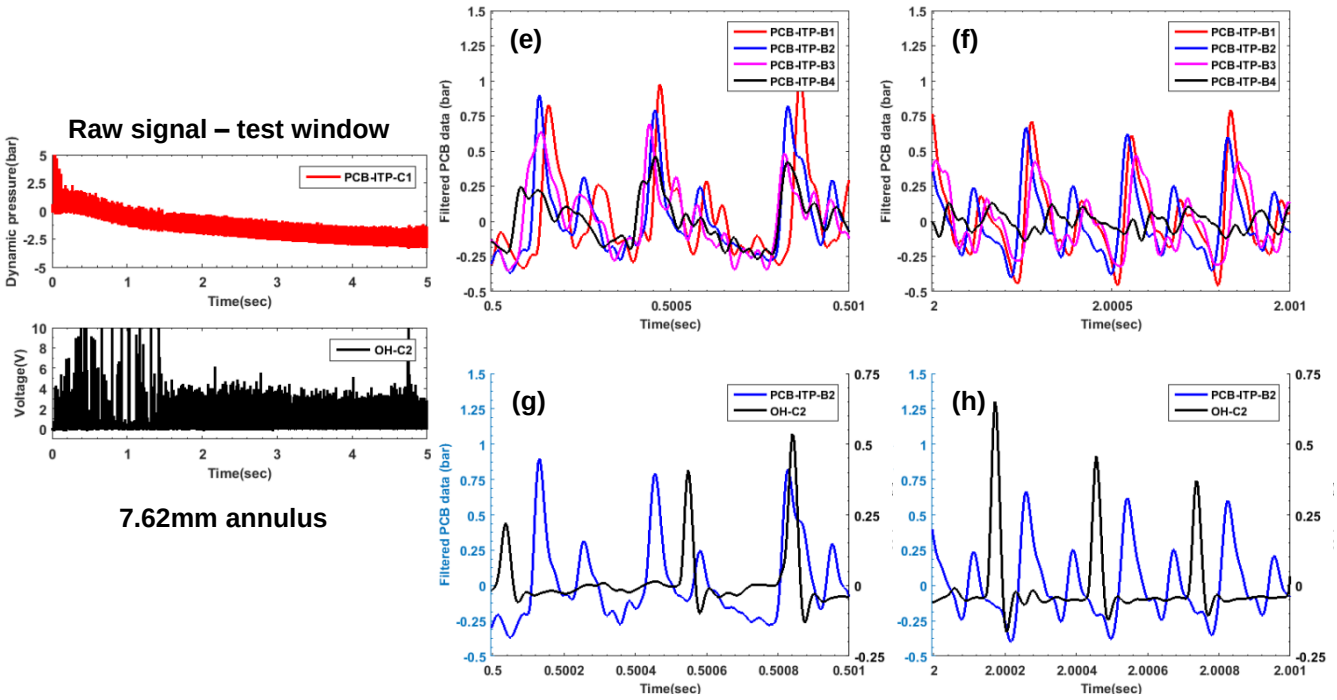

Figure 9: Effect of annulus gap width – raw signal (PCB-C1 and OH*-C2) measured during full test window and close-up view of dynamic pressure trace measured at B1, B2, B3 and B4 and B2, OH* signal respectively at different instants (t1=0.5s and t2=2s) during the test window under conditions as shown in Fig. 8

Similar to Fig. 6, Fig. 8 shows corresponding spectrogram plots of the filtered dynamic pressure trace and OH* chemiluminescence data filtered ((a)-(b), (d)-(e)), along with variation of the dominant frequency mode during the test window ((c), (f)). The spectrogram plots do not exhibit any abrupt mode change in detonation wave propagation. However, it is observed that during the initial period after start up the detonation wave has not achieved a stable mode of propagation which is evident from a diffused and broadened spectrogram signal. This instability could arise due to inhomogeneity in mixing within the combustor annulus at higher preheat temperatures after detonation initiation as it took almost 0.7s for 5.08mm annulus and ~1.5s for 7.62mm annulus for the detonation wave to stabilize. However, after the initial unstable characteristics both annulus sizes exhibit detonation wave and reaction front decoupling as seen from the dominant frequency distribution (Fig. 8(c), (f)). The unstable detonation wave most likely operating in a collision mode with a frequency equivalent to a one wave operation during the initial phase bifurcated into a steadier de-coupled detonation wave where a single detonation wave could be accompanied by a pure shock wave intermittently converting into a detonation front and vice versa.

This behavior is further explored in Fig.9, where similar to Fig. 7, two different time windows (t1=0.5s and t2=2s) were selected from the test duration and filtered PCB data (B1-B4) along the axial direction and OH* data (C2) along the circumferential direction is plotted w.r.t time. It is observed that the raw dynamic pressure data qualitatively shows lower amplitude oscillation for larger annulus similar to combustion air temperature of 65°C with hydrogen-air only. The trends obtained are fairly similar as was observed in case of hydrogen-air operation comparing the two annulus gap sizes in Fig.7. Both annulus sizes show multiple secondary peaks in between dominant ones with lesser time lag between B1-B2 peaks for the larger one. The amplitudes of peak pressure oscillation are fairly comparable between both cases except for t2=2s, where the larger annulus values seem to be slightly lower. The fact that the detonation waves could be operating in a collision mode during the initial period is also evident from disordered arrangement of pressure peaks w.r.t. the OH* signal as seen in Figs. 9(c), (g). The random appearance of OH* peaks w.r.t. the PCB-B2 peaks suggests that the reaction front could be decoupled from the detonation waves after collision, forming new shock waves which propagate within the chamber. These shock waves may ultimately transition into a detonation wave and collide with each other again to develop a continuous formation and destruction pattern. At t2=2s, the double peaks in PCB data appear for both annulus gap sizes, however the OH* signal peaks are more ordered and appear in a regular period interval w.r.t. the pressure peaks. This suggests that the RDC is operating in a homogenous rotational mode with one detonation

wave and an accompanying secondary shock wave. Overall, it can be observed that the annulus gap size has no significant effect on the RDC characteristics when operated at elevated combustion air temperature (121°C) with hydrogen-NG fuel blend (5% NG).

Effect of air preheat on RDC performance for larger annulus gap size (7.62mm) with and without natural gas addition

Figure 10 represents wave speed variation w.r.t. equivalence ratio in traditional box and whisker plot format calculated at the detonation plane (C1) using high frequency dynamic pressure transducer data. The wave speed distributions shown in the box plots in Fig.10 are calculated from the fundamental frequencies obtained from FFT analysis of the PCB data for the entire test duration. Theoretical detonation wave speeds (CJ values) are shown for reference and calculated using SDToolbox [23] for a specific inlet and mixture condition and experimentally measured wave speeds are adjusted w.r.t. to the corresponding CJ speed to account for the number of waves. These case studies are performed for larger annulus gap width (7.62mm) where, the total flow rate to the RDC was kept constant at $0.47 m^3/s$ at all combustion air temperatures and equivalence ratios while the combustor operating at pre-combustion pressures near atmospheric.

The idea behind representing wave speed distribution in the form of box and whisker plots is primarily motivated from the variability in RDC characteristics under similar conditions as well as the different detonation wave operating modes observed during a single test run (up to ~ 6s). This accounts for the wave speed adjustment due to mode shift or bifurcation behavior that can be observed in a single test window. This plot reveals a realistic quantitative description of the unsteady behavior of detonation waves and associated RDC performance. This was important to highlight as experiments performed in an uncooled RDC are typically short duration in nature and vary from a few milliseconds to several seconds. Though a physical time frame of several hundred milliseconds is sufficient to attain a stable or quasi-stable detonation, the RDC has not attained thermal equilibrium. Therefore, it is important to report the entire range of observed operating modes not only for different operating conditions, but also for the entire duration of a specific operating condition when presenting data from an uncooled RDC. These unsteady trends could be ignored and a steady state operational characteristic would be more appropriate only in the context of a cooled RDC after reaching thermal equilibrium. It can be observed from Fig.10 that for hydrogen-air mixture (10(a)-(c)) the wave speed increases gradually with increase in fuel content and the variation is fairly small at all equivalence ratios except at lean condition (phi ~0.6-0.65) with combustion air temperatures of 65°C and 121°C respectively. This characteristic is expected under lean conditions, where the detonation wave fronts primarily exhibit random collision and bifurcation modes due to spatial inhomogeneity of the mixture. At 204°C, the higher combustion air temperature can influence the wave performance by increasing the reactivity of the mixture and thereby resulting in a faster and stable propagation velocity along with faster transition to detonation. Since the total flow rate for all the cases remain constant, fuel-air mixing inside the combustor is fairly uniform between different equivalence ratios, as opposed to a fixed air flow rate. Higher combustion air temperatures though favors multiple number of waves with reduced instability, however, can also increase deflagration losses that account for larger difference between the theoretical CJ speed and the experimental measured speed for a specific equivalence ratio. Overall, the global wave speed distribution trends w.r.t. equivalence ratio measured for hydrogen-air mixture under varying air preheat levels is consistent with previously published study [30].

Adding natural gas to the hydrogen fuel stream and obtaining sustained detonation under nominal operating condition (65°C) is one of the most important findings of this experimental study reported in this paper. It is important to mention here that for the 7.62mm annulus configuration, experiments were performed at 5%-10%-12.5%-15% natural gas concentration in the binary fuel mixture. However, for all cases including and above 10%, attempts to initiate or sustain detonation was not successful leading to detonation blow out or unsteady deflagration. Therefore, all cases shown in Figs. 10(d)-(f) contain 5% natural gas by volume with a balance of hydrogen. It has also been mentioned that successful detonation could not be achieved even with the slightest amount of natural gas for 5.08mm annulus gap RDC configuration at a combustion air temperature of 65°C. It is observed that the wave speed variation is significantly higher with addition of natural gas especially at equivalence ratio of equal to or greater than 0.8. Furthermore, these conditions also exhibit intermittent to complete detonation blow out during the initial phase or later in the test window. Detailed insight of these characteristics will be discussed later in this section. The primary reason for being able to initiate and sustain detonation with natural gas-hydrogen mixture even in an unstable mode at a combustion air temperature of 65°C could be attributed to a larger annulus gap size (compared to 5.08mm) that may be sufficient enough to accommodate the cell size of the specific mixture condition. Typically, large differences in detonation cell sizes for hydrogen and natural gas contribute towards this instability. At higher combustion air temperatures, reactivity of natural gas increases thereby reducing the wave speed variability. However the effect of instability is still observed near stoichiometric mixture at 121°C. When compared with pure hydrogen operation at similar combustion air temperatures the overall wave speeds are much lower in presence of natural gas due to lower detonability of the mixture. At an air temperature of 204°C, hydrogen-natural gas mixture wave speed characteristics are almost similar to that of 121°C with slightly higher median speed and reduced variability near stoichiometric operation.

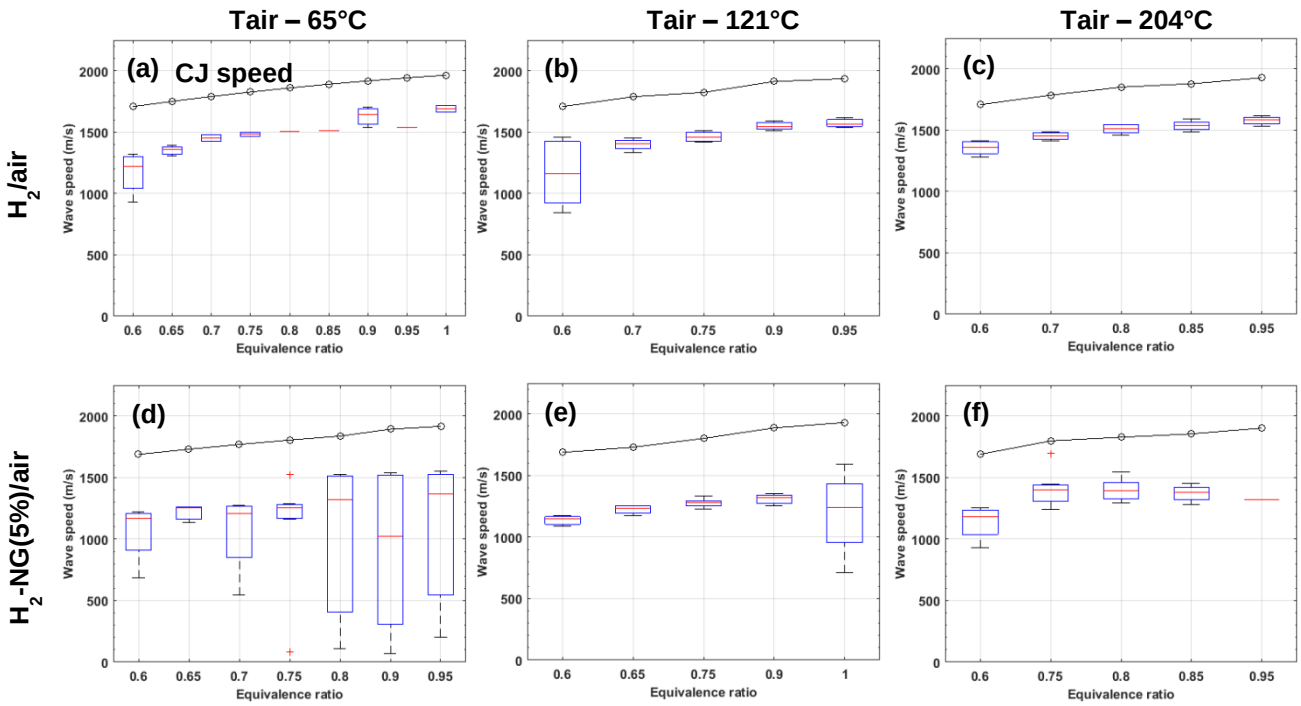

Figure 10: Effect of air preheat on RDC operational wave speed w.r.t. equivalence ratio at ambient initial combustor pressure, total flow rate of 0.47m^3/s with hydrogen-air and with natural gas addition at 5% concentration for 7.62mm annulus gap

Figure 11 shows corresponding spectrogram plots of dynamic pressure, OH* with dominant frequency distribution over time at stoichiometric mixture comparing pure hydrogen and hydrogen-natural gas (5%) operation at nominal and elevated combustion air temperatures of 65°C and 204°C respectively, atmospheric pre-combustion pressure, 7.62mm annuls gap width and a total flow rate of 0.47m^3/s. It can be noted that during the initial phase up to 1s of igniting the mixture, the frequency oscillation amplitudes are much larger in the presence of natural gas compared to pure hydrogen. Furthermore, during this initial phase around 0.5s of the test run, the pressure trace as well as the OH* signal exhibit detonation blow out and re-initiation in multiple occasions as highlighted within region A in Fig. 11. At the nominal combustion air temperature (65^{o}C) there is possibly not sufficient reactivity in the natural gas-hydrogen mixture and therefore not only it is harder to initiate detonation, but detonation once achieved becomes difficult to sustain. However with continuous feed supply, multiple detonation fronts colliding randomly generate greater heat release into the mixture. Wall thermal effects can also influence the deflagration regions transition to detonation faster accompanied by shock waves produced from collision of detonation waves or reflection from main wave front. Hydrogen-air mixture on the other hand initiates detonation much rapidly and operates in a steady and stable homogeneous rotating mode. The dominant frequency distribution clearly shows presence of a shock wave in addition to the original detonation wave front for both pure hydrogen and while operating with of natural gas. During the initial phase (0.4s-0.6s) in presence of natural gas, the fundamental frequency obtained from OH* signal is larger compared to PCB-C1. This may be attributed due to strong deflagration of the unreacted mixture in the fill zone or within the combustor arising out of collision of the unstable detonation wave fronts. The instability in detonation wave initiation, propagation, blow out and re-ignition is clearly depicted in Fig. 12 which shows a comparison of startup operation window between pure hydrogen (left) and in presence of natural gas (right). It is clearly evident from Fig.12 that a significant amount of time (Δt_F ~ 0.17s) is required to obtain steady detonation in case of natural gas mixed with hydrogen after the initiator is fired. Within this time window, several blow out and re-ignition events happen with the most pronounced one being between 0.14s-0.17s. Whereas, in case of pure hydrogen the detonation initiation is almost instantaneous.

Figure 11 also presents detonation wave front characteristics obtained from the experimental data similarly for combustion air temperature of 204°C. At higher air temperatures several important aspects can be readily identified – first, for hydrogen-air mixture the detonation initiation is instantaneous, however in presence of natural gas Δt_F ~2s after initiator is fired for the present case study.

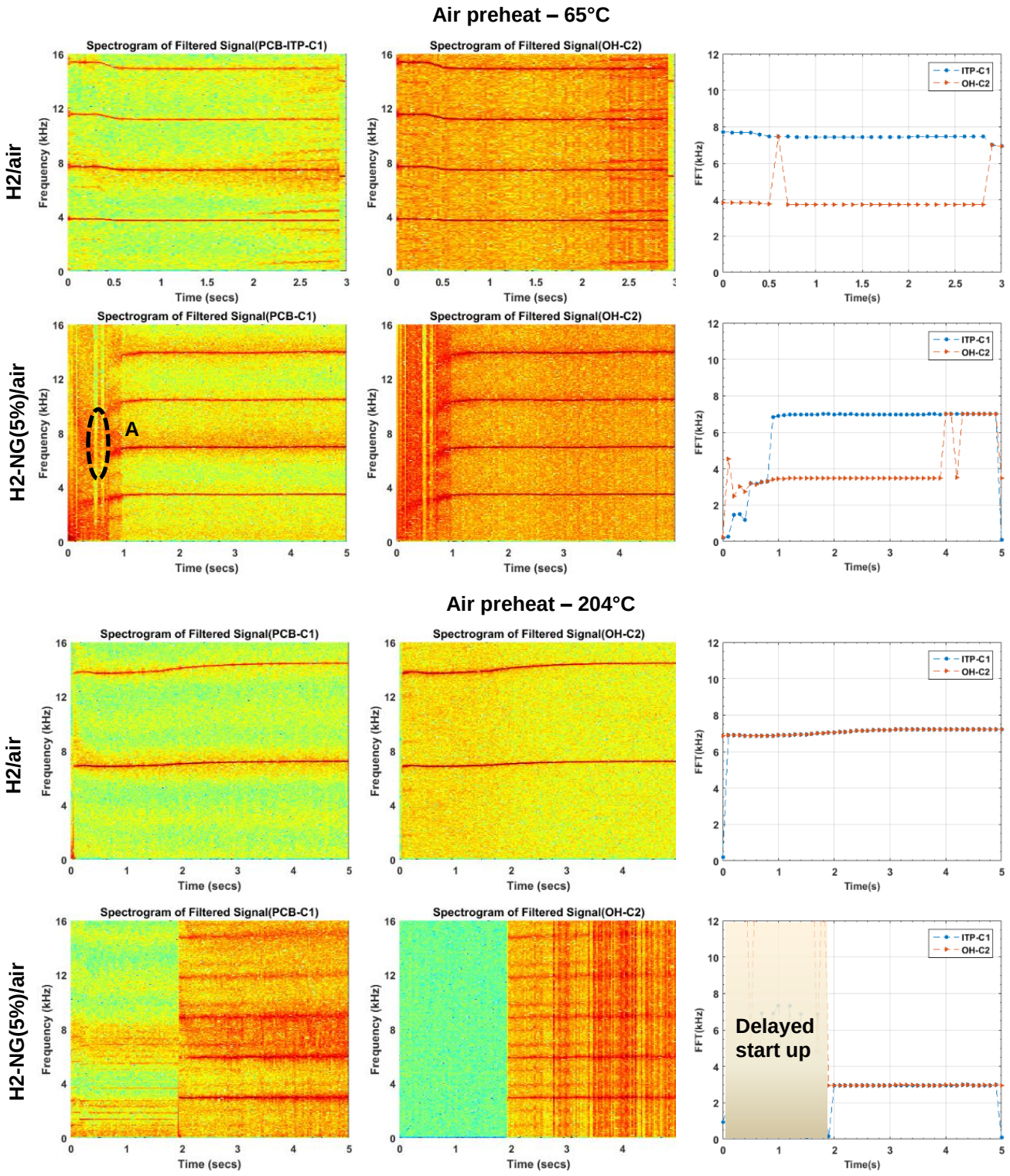

Figure 11: Effect of air preheat (65°C/204°C) on RDC performance for pure hydrogen and hydrogen-natural gas blend air operation at NG content = 5%, phi~1.0, total flow rate ~ 0.47m^3/s, 7.62mm annulus gap, and near ambient exhaust pressure – Spectrogram of ITP-C1 (left) and OH* signal (middle) filtered between 100Hz and 20kHz, and dominant frequency distribution w.r.t. test duration obtained from PCB-C1 and OH* (right)

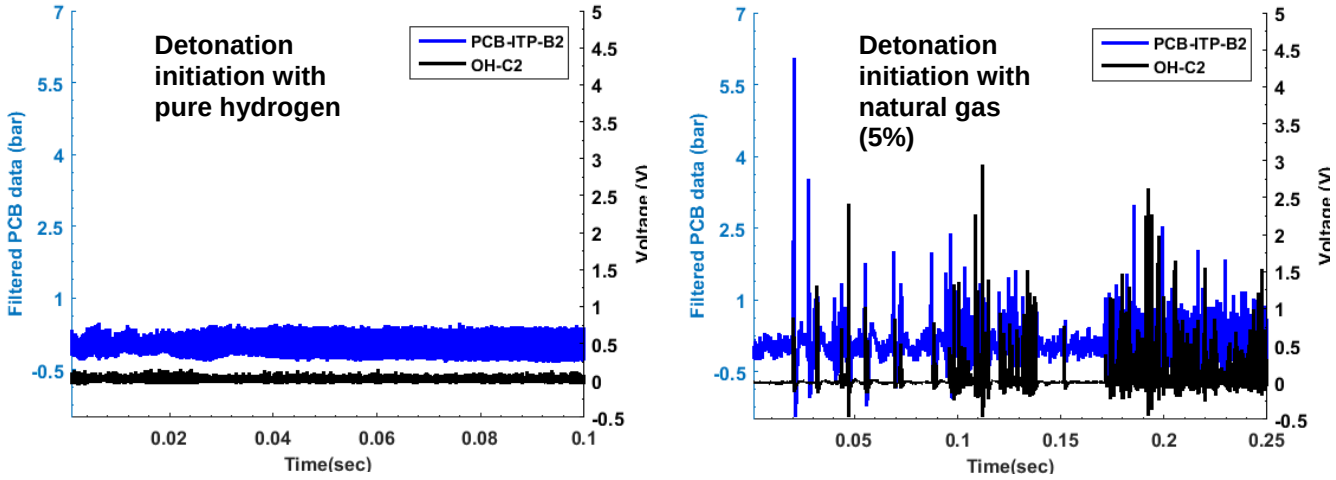

Figure 12: Detonation initiation time for pure hydrogen and hydrogen-natural gas blend air operation at, NG = 5%, phi~1.0, air preheat of 65°C, total flow rate ~ 0.47m^3/s, 7.62mm annulus gap, and near ambient exhaust pressure (filtered PCB-B2 with OH* signal)

The startup time is expected to be longer when operated at lean mixture condition. Second, hydrogen-air mixture exhibits a much cleaner spectrogram plot for both C1 and OH* with peaks ~7kHz, whereas in presence of natural gas the spectrogram plots are much more diffused and broadened around the dominant frequency. This indicates not only a decrease in wave speed, but also illustrates the presence of instability with a broader frequency distribution. This can be a result of inception of collisional modes as well as random detonation structures being created in a non-uniform manner. Finally, complete coupling between shock wave and the reaction fronts in the detonation wave propagation is another distinctive feature for both pure hydrogen and natural gas blend with lower frequency operation as evident from dominant frequency distribution comparison between PCB at C1 and OH* at C2.

Effect of Cell Size on Detonability

As a result of the challenges experienced in achieving stable detonation with the addition of natural gas, some further discussion of detonability limits is warranted. By using the hydrogen-methane cell size data from [19], along with extrapolation to consider the effects of elevated initial temperature, representative cell sizes were estimated for the experimental conditions considered in this paper. The extrapolation approach was similar to that of [28], in which a linear fit of a log-log plot of cell size versus temperature was used to estimate the corresponding temperature reduction. Ref. [28] presented two linear fits for pure methane and pure hydrogen fuels. In general, the reduction in cell size with increasing temperature was lower for methane compared to hydrogen. As a result, the linear fit slope was estimated for the hydrogen-methane mixtures by interpolating between that of pure methane and pure hydrogen from [28].

Cell size (λ) was normalized with respect to two characteristic dimensions associated with RDC geometry: annulus gap width (w) and fill height (h). In the calculation of fill height (Eq. 1), combustion air temperature and overall reactant composition (hydrogen-natural gas-air) were considered in computing ρ_{mix}.

For the conditions and RDC configurations examined in this work, the ratio of cell size to annulus gap width (λ/w) remained greater than 1. As such, it is hypothesized that transverse waves occur primarily in the axial direction, within the fill height (i.e. along the wave front). The addition of natural gas inherently changes the detonation cell size and changes to the RDC gap width affect fill height. As such, this provides an opportunity to examine trends in the context of noted instabilities or detonation failure.

A general comparison of the computed λ/h values was performed for volume fractions of natural gas in fuel ranging from 0% (hydrogen only) to 20%. Relevant to the data presented in this paper, reactant temperatures were considered between 65°C and 204°C, and annulus gap sizes of 5.08mm and 7.62mm. It is clear from the experimental data in Fig. 6 and Fig. 8, that depending on conditions, 1-3 waves may be present in the RDC. As such, 1, 2, and 3 wave systems were considered, corresponding to measured operational frequencies of 4000, 7000, and 11000 Hz.

In Fig. 13, the operational points of 65°C, 121°C, and 204°C, as well as 5% natural gas addition, are highlighted by dashed lines. In this form, any contour greater than 1 corresponds to a detonation cell size which is greater than the fill height. Lower values correspond to a greater number of

cells within the wave front, perhaps implying improved stability.

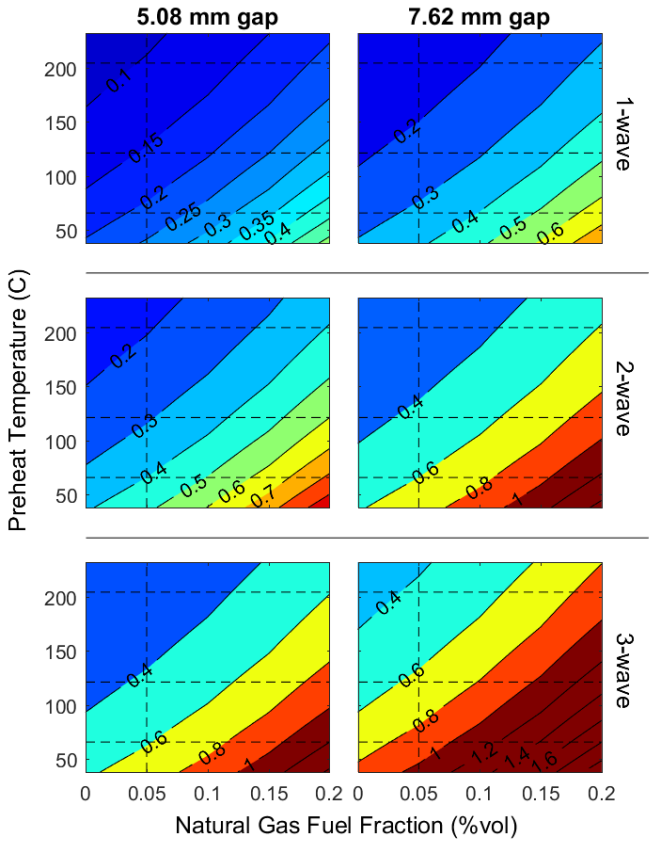

Figure 13: Theoretical ratio of cell size to fill height vs. natural gas addition, preheat temperature for 5.08mm and 7.62mm annulus gap size and 1, 2, and 3 wave systems, air flow rate 0.35m^3/s, phi=0.95

In Fig. 6, it can be seen that two waves were initially generated for the 5.08mm gap (f_{RDC}~7000 Hz), while only one wave is seen for the 7.62mm gap (f_{RDC}~4000 Hz). Later, the smaller gap transitions to 3-wave operation (f_{RDC}~11000 Hz), while the larger gap transitions to a 2-wave. If the conditions of Fig. 6 are examined in Fig. 13 (0% natural gas, 65°C), it can be seen that for the 5.08mm gap, a 2-wave system would correspond to λ/h~0.3, while a 3-wave would be ~0.5. Similarly, for the 7.62mm gap, a 1-wave system would correspond to λ/h ~0.28, while a 2-wave would be ~0.5. This may point to some λ/h threshold necessary for stable detonative operation, perhaps near ~0.33, or 3 cells within the wave front.

In each case, later in the run a transition is seen to a higher number of waves. Undoubtedly, heating of the RDC has occurred in each instance. If one considers Fig. 13 with an additional ~38°C of reactant preheating, the 3-wave and 2-wave λ/h values for the 5.08mm and 7.62mm gaps, respectively, drop below ~0.3. Additionally, greater preheating of the 7.62mm gap serves to reduce the λ/h more quickly than for the 5.08mm gap, supporting the more rapid transition to a higher number of waves in Fig. 6.

Considering Fig. 8, a similar relationship can be seen (minus the wave number transition). For the 1-wave system (5% natural gas, 121°C), λ/h~0.16 for the 5.08mm gap and ~0.23 for the 7.62mm gap as shown in Fig. 13. But in general, the frequency distributions are much noisier in Fig. 8, showing some near 2-wave frequency components (Fig. 8 d and h). In Fig. 13, moving to a 2-wave system corresponds to λ/h~0.28 and 0.4, for the 5.08mm and 7.62mm gaps, respectively. As these are somewhat near the values seen in Fig. 6 for a 2-wave system, it may imply the formation of a second wave to be immenent.

It must be acknowledged that many prior works involving cell size and detonability limits were performed in the context of a simplified experimental configuration and largely homogeneous reactant mixture. While the approach of relating detonability limits to cell size is expected to remain valid in an RDC, the driving geometric relationships are unknown. Additionally (and perhaps most important) is the dynamic and heterogeneous nature of the medium in which the detonation propagates within an RDC. This may result in significant variation in cell size both temporally and spatially due to mixing and injector dynamics. Exactly how this relates to device operability and overall detonation stability has yet to be understood. As such, the specific numeric values of λ/h should not be emphasized due to the high expected uncertainty in cell size estimates and simplified fill height estimation. Instead, focus should be placed on the general trends and how they relate to observed instabilities in the RDC.

CONCLUSIONS

Experimental data characterizing performance of an air breathing RDC operating in presence of natural gas in the fuel stream with hydrogen under different annulus gap size , varying air inlet temperature and pre-combustion pressure near atmospheric is reported in this study. The operational modes and regions of instability have been discussed in detail. One of the major findings has been the ability to sustain detonation in the larger annulus gap size (7.62 mm) compared to the small gap size (5.08 mm) when fueled with a hydrogen-natural gas-air mixture at similar operating conditions.. This phenomenon may be correlated with the disparity between the detonation cell sizes of hydrogen and natural gas, although additional testing is required. The detonation wave speed variability is found to be largest near stoichiometric operation with a reduced inlet air temperature and in the presence of natural gas. The varying inlet air temperature influences the shock wave reaction front coupling where, higher temperatures appear to accelerate the deflgration to detonation transition.

While the data presented here paint a complex picture for RDC operation with natural gas-hydrogen blends with air as oxidizer, several general conclusions from this study can be made:

1. Adding a small amount of methane to a hydrogen base fuel has a profound negative impact on the detonation limits and propagation stability when operating at near atmospheric pre-combustion pressures. For the current configuration, a maximum of about 5% natural gas content in the fuel was the limit of stable detonation in the current RDC geometry (larger annulus gap size – 7.62mm). This is likely due to the increase in induction time associated with the slower methane kinetics.
2. Elevating the reactant temperatures (only air in this study) helps to offset the addition of methane by decreasing the induction time which improves the stability of the detonation wave. This may also have a positive impact on reactant mixing. It is anticipated that operating at higher pre-combustion pressures would also improve detonation wave stability although this was not examined in this study.
3. Increasing the gap size generally allows for stable detonation with higher methane contents although this was found to be condition specific. Inlet air temperature, pre-combustion pressure and equivalence ratio all are important parameters to be taken into consideration. It is hypothesized that the larger gap size allows for more transverse wave formation in the detonation front which helps to stabilize the detonation wave.
4. Finally, the RDC injector configuration and injection scheme reported in this study is not optimized for natural gas operation. The current geometry was designed specifically for achieving sustained detonation in hydrogen-air mixtures. Therefore, when design changes are considered for favorable operation of pure natural gas or blends, changing the annulus gap size alone may not be sufficient. Modification of the injection scheme may also play a significant role in improving mixing. Looking at the detonation start up trends in this study, it can be recommended that for steady long duration operation the RDC be initiated with hydrogen-air mixture with subsequent addition of natural gas after a stable detonation wave is achieved.

ACKNOWLEDGEMENTS

This work was performed in support of the National Energy Technology Laboratory's ongoing research under the RSS contract 89243318CFE000003.

DISCLAIMER

The project was funded by the Department of Energy, National Energy Technology Laboratory, an agency of the United State Government, through a support contract with Leidos Research Support Team (LRST). Neither the United States Government nor any agency thereof, nor any of their employees, nor LRST, nor any of their employees, makes any warranty, expressed or implied, or assumes any legal liability or responsibility for the accuracy, completeness, or usefulness of any information, apparatus, product, or process disclosed, or represents that its use would not infringe privately owned rights. Reference herein to any specific commercial product, process, or service by trade name, trademark, manufacturer, or otherwise, does not necessarily constitute or imply its endorsement, recommendation, or favoring by the United States Government or any agency thereof. The views and opinions of authors expressed herein do not necessarily state or reflect those of the United States Government or any agency thereof.

REFERENCES

[1] Patel, S., 2018, "GE HA Turbine Snags Another World Record for CCGT Efficiency," Power Mag.

[2] Anand, V., St. George, A., Driscoll, R., and Gutmark, E., 2015, "Characterization of Instabilities in a Rotating Detonation Combustor," Int. J. Hydrogen Energy, **40**(46), pp. 16649–16659.

[3] Anand, V., St. George, A., Driscoll, R., and Gutmark, E., 2016, "Investigation of Rotating Detonation Combustor Operation with H2-Air Mixtures," Int. J. Hydrogen Energy, **41**(2), pp. 1281–1292.

[4] Zhang, Y., Xu, A., Zhang, G., Zhu, C., and Lin, C., 2016, "Kinetic Modeling of Detonation and Effects of Negative Temperature Coefficient," Combust. Flame, **173**, pp. 483–492.

[5] Ma, Z., Zhang, S., Luan, M., Yao, S., Xia, Z., and Wang, J., 2018, "Experimental Research on Ignition, Quenching, Reinitiation and the Stabilization Process in Rotating Detonation Engine," Int. J. Hydrogen Energy.

[6] Anand, V., George, A., Driscoll, R., and Gutmark, E., 2016, "Analysis of Air Inlet and Fuel Plenum Behavior in a Rotating Detonation Combustor," Exp. Therm. Fluid Sci., **70**, pp. 408–416.

[7] Li, Y., Wang, Y., Wang, J., and Li, Y., 2014, "Detonation Instability of Continuously Rotating Detonation Engines for H 2 -Air Mixture," Int. Invent. J. Eng. Sci. Technol., **1**(1), pp. 1–7.

[8] Anand, V., St. George, A., and Gutmark, E., 2017, "Amplitude Modulated Instability in Reactants Plenum of a Rotating Detonation Combustor," Int. J. Hydrogen Energy.

[9] George, A. S., Driscoll, R., Anand, V., and Gutmark, E., 2016, "On the Existence and Multiplicity of Rotating Detonations," Proc. Combust. Inst., **11**(0), pp.

1–8.
[10] Bluemner, R., Bohon, M. D., Paschereit, C. O., and Gutmark, E. J., 2018, "Single and Counter-Rotating Wave Modes in an RDC," *2018 AIAA Aerospace Sciences Meeting*.
[11] Zahn, A., Knight, E., Anand, V., Jodele, J., and Gutmark, E. J., 2018, "Examination of Counter-Rotating Detonation Waves Using Cross-Correlation," *2018 Joint Propulsion Conference*.
[12] Anand, V., St. George, A., Driscoll, R., and Gutmark, E., 2016, "Longitudinal Pulsed Detonation Instability in a Rotating Detonation Combustor," Exp. Therm. Fluid Sci., **77**, pp. 212–225.
[13] Bull, D.C.; Elsworth, J.E.; Shuff, P. J., 1982, "Detonation Cell Structures in Fuel/Air Mixtures," Combust. Flame, **45**, pp. 7–22.
[14] Guirao, C. M., Knystautas, R., and Lee, J. H., 1989, *A Summary of Hydrogen-Air Detonation Experiments*.
[15] Wilhite, J., Driscoll, R. B., St. George, A. C., Ganesh Kumar, V. A., and Gutmark, E. J., 2016, "Investigation of a Rotating Detonation Engine Using Ethylene-Air Mixture," *54th AIAA Aerospace Sciences Meeting*, pp. 1–7.
[16] Schwer, D. A., and Kailasanath, K., 2011, "Effect of Inlet on Fill Region and Performance of Rotating Detonation Engines," 47th AIAA/ASME/SAE/ASEE Jt. Propuls. Conf. Exhib., (August), pp. 1–17.
[17] Kaneshige, M., and Shepherd, J. E., 1997, "Detonation Database," Galcit, (July), pp. 130–131.
[18] Zipf, R. K., Gamezo, V. N., Sapko, M. J., Marchewka, W. P., Mohamed, K. M., Oran, E. S., Kessler, D. A., Weiss, E. S., Addis, J. D., Karnack, F. A., and Sellers, D. D., 2013, "Methane-Air Detonation Experiments at NIOSH Lake Lynn Laboratory," J. Loss Prev. Process Ind., **26**(2), pp. 295–301.
[19] Sorin, R., Bozier, O., Zitoun, R., and Desbordes, D., 2009, "Deflagration to Detonation Transition in Binary Fuel H 2 / CH 4 with Air Mixtures," Int. Colloq. Dyn. Explos. React. Syst., pp. 6–9.
[20] Anand, V., St. George, A., Farbos de Luzan, C., and Gutmark, E., 2018, "Rotating Detonation Wave Mechanics through Ethylene-Air Mixtures in Hollow Combustors, and Implications to High Frequency Combustion Instabilities," Exp. Therm. Fluid Sci., **92**(October 2017), pp. 314–325.
[21] Wang, Y., Le, J., Wang, C., and Zheng, Y., 2018, "A Non-Premixed Rotating Detonation Engine Using Ethylene and Air," Appl. Therm. Eng., **137**(April), pp. 749–757.
[22] Zhong, Y., Jin, D., Wu, Y., and Chen, X., 2018, "Investigation of Rotating Detonation Wave Fueled by 'ethylene-Acetylene-Hydrogen' Mixture," Int. J. Hydrogen Energy, **43**(31), pp. 14787–14797.
[23] Shepherd, J. E., 2018, "Shock & Detonation Toolbox - Cantera 2.1," http://shepherd.caltech.edu/EDL/public/cantera/html/SD_Toolbox/.
[24] Schwer, D. A., and Kailasanath, K., 2017, "Assessment of Rotating Detonation Engines with Fuel Blends," *53rd AIAA/SAE/ASEE Joint Propulsion Conference*, pp. 1–16.
[25] Bykovskii, F. a, Zhdan, S. a, and Vedernikov, E. F., 2018, "Continuous Detonation of Methane/Hydrogen–Air Mixtures in an Annular Cylindrical Combustor," Combust. Explos. Shock Waves, **54**(4), pp. 472–481.
[26] Welch, C., Depperschmidt, D., Miller, R., Tobias, J., Uddi, M., Agrawal, A. K., and Lowe, S., 2018, "Experimental Analysis of Wave Propagation in a Methane-Fueled Rotating Detonation Combustor," *Proceedings of ASME Turbo Expo 2018: Turbine Technical Conference and Exposition*, June 11-15, 2018, Oslo, Norway, pp. 1–11.
[27] Tobias, J., Depperschmidt, D., Welch, C., Miller, R., Uddi, M., Agrawal, A. K., and Jr, R. D., 2018, "OH* CHEMILUMINESCENCE IMAGING OF THE COMBUSTION PRODUCTS FROM A METHANE-FUELED ROTATING DETONATION ENGINE," *Proceedings of ASME Turbo Expo 2018 Turbomachinery Technical Conference and Exposition*, June 11-15, 2018, Oslo, Norway, pp. 1–14.
[28] Walters, I. V., Journell, C., Lemcherfi, A., Gejji, R., Heister, S. D., and Slabaugh, C. D., 2018, "Experimental Investigation of a Piloted, Natural Gas-Air Rotating Detonation Wave Combustor," *2018 Joint Propulsion Conference*.
[29] Naples, A., Hoke, J. L., and Schauer, F. R., 2018, "Quantification of Infinite Line Pressure Probe Response to Shocks and Detonation Waves," *2018 AIAA Aerospace Sciences Meeting*, pp. 1–12.
[30] Roy, A., Ferguson, D., Sidwell, T., O'Meara, B., Strakey, P., Bedick, C., and Sisler, A., 2017, "Experimental Study of Rotating Detonation Combustor Performance under Preheat and Back Pressure Operation," *AIAA SciTech Forum - 55th AIAA Aerospace Sciences Meeting*.